Geopersia **6** *(2), 2016, PP. 243-264*

Fractal dimension and earthquake frequency-magnitude distribution in the North of Central-East Iran Blocks (NCEIB)

Nasser Naimi Ghassabian [1,2]*, Mohammad Mahdi Khatib [1], Hamid Nazari [3], Mahmoud Reza Heyhat [1]
[1] *Department of Geology, Faculty of Earth Sciences, University of Birjand, Birjand, Iran*
[2] *Geological Survey of Iran, Northeast Territory Mashhad, Iran*
[3] *Research institute for Earth sciences, Geological Survey of Iran*
**Corresponding author, e-mail: naser.naimi@birjand.ac.ir*
(*received: 04/05/2016 ; accepted: 29/08/2016*)

Abstract
The Gutenberg–Richter parameters (*a* and *b*), fractal dimension (D_C), and relationships between these parameters are calculated for different regions of the North of Central-East Iran Blocks (NCEIB). The whole examined area (between 34˚-36˚ N and 55˚-61˚ E) is divided into 55 equal square grids. Both the *a* and *b* values for the frequency-magnitude distribution (FMD) and the fractal dimension (D_C) are investigated simultaneously from 55 equal square grids. By using the completeness earthquake dataset for earthquakes of the instrumental period from 1976 to 2015, it is concluded that calculated values of *a*, *b* and D_C imply variations of seismotectonic stress. The most vulnerable regions for occurrence of the large earthquakes in the NCEIB considering the computed lowest *b*-values and the highest D_C -values. The relationships among D_C *-b* and D_C - *(a/b)* are used to classify the level of earthquake hazards for individual seismic source zones, in which the calibration curves illustrate a positive correlation among the D_C and *b* values and also a positive correlation among the D_C and *a/b* ratios having similar regression coefficients (R2 = 0.80 to 0.87) for both regressions. It is observed that the relationship among *a/b* and D_C may be used for evaluation of seismicity and earthquake hazard assessment because of the high value for correlation coefficients and limited scattering of the calculated parameters.

Keywords: *seismicity; frequency-magnitude distribution; fractal dimension; Central-East Iran Blocks.*

Introduction

Iran is located in between relatively rigid, aseismic blocks: Arabia to the southwest, The Turan Shield (belonging to the Eurasian plate) to the northeast and the Hellmand block (Eurasian plate) to the east (Jackson & McKenzie 1984; Jackson *et al.* 1995) (Fig. 1).

The active tectonics of Iran is dominated by the northward motion of the Arabia plate relative to Eurasia. The earthquake distribution indicates that the convergence is accommodated by a mixture of thrust and strike-slip faulting inside Iran. Therefore, this convergence is absorbed by shortening, thickening of the crust, and strike-slip motions on major faults. The characteristic feature of the convergence along Iran's southern border is the longitudinal variation in style, from continental collision in the west to oceanic subduction in the east (east of 58̊ E). In the west, shortening is mainly accommodated in the Zagros and Alborz-Caucasus mountain belt, while east of 58̊ E most of the convergence is accommodated by the Makran subduction zone (Vernant *et al.,* 2004 a, b), with the remaining shortening taken up by the Kopeh-Dagh and other mountain ranges in NE Iran.

The Central-East Iranian Blocks (CEIB) is an important individual continental block within the collision zone between the Arabia and Eurasia, which affects the distribution of strain in the eastern part of the Iranian-Turkish plateau (Javadi *et al.,* 2013; Naimi-Ghassabian *et al.,* 2015). The CEIB deformation pattern is imposed by the NS shear resulting from the E-W variation in accommodation of the convergence. A major part of this shear is absorbed on the north of Central-East Iranian Blocks (NCEIB), boundaries, while the residual NS shortening NCEIB provides the boundary conditions for the Kopeh-Dagh and Eastern Alborz present-day deformation. These latter deformation patterns fainally constrain the present kinematics of the South Caspian Basin in the west.

Our study area is situated in the NCEIB, between 34˚-36˚ N and 55˚-61˚ E, which is the transfer zone between the northern deforming zones (i.e., Alborz, Kopeh-dagh, Binalud mountain ranges and Sabzevar domain) and a southern domain with NS fault systems (Naimi-Ghassabian *et al.,* 2015). These zones are separated by the Doruneh fault system (DFS) (e.g., Tchalenko *et al.,* 1973; Farbod *et al.,* 2011) which precludes their direct structural connection. The DFS extends for ~900 km between the Anarak area of Central Iran and the Herat area in western Afghanistan. The DFS is also considered as an important structure in the Arabia–Eurasia collisional zone, which forms the northern margin of the independent CEIB (Javadi *et al.,* 2013).

The tectonically active DFS (Fig. 2) has not shown any instrumental or historical earthquakes of magnitudes M ≥ 6 (e.g. Ambraseys & Melville 1982), suggesting that it may produce earthquakes of large magnitudes (M ≥ 7.5) (Berberian and Yeats 1999; Fattahi *et al.,* 2007) with a long return period capable of developing a high seismic hazard potential for the region.

Importance of understanding the Gutenberg–Richter (G–R) relationship and fractal dimension of seismicity in assessment of the earthquake hazard for a tectonically active region has been highlighted by Bayrak & Bayrak (2012). Seismicity parameters *a* and *b* value, and fractal dimension, *Dc* may be used as quantitative approaches to analysis of seismicity in a region The *a* and *b* values are obtained from frequency magnitude distribution analyzed by the Gutenberg–Richter (G–R) relationship. The *Dc* value can be estimated using the correlation dimension. The relationships among the *b* and *Dc* values of earthquakes has been extensively discussed during the last three decades (e.g. Aki, 1981; King, 1983; Turcotte 1986; Hirata 1989; Wang 1991,1996; Öncel *et al.,* 1996; Henderson *et al.,* 1999; Legrand 2002; Wyss et al. 2004; Mandal & Rastogi 2005). Either positive (e.g. Guo & Ogata 1995; Legrand 2002; Pascua *et al.,* 2003; Öncel & Wilson 2004) and negative (e.g. Hirata 1989; Henderson *et al.,* 1994; Öncel *et al.,* 1996; Wang & Lee 1996) correlations among the two above-mentioned scaling exponents have been suggested and discussed in the literature. In some cases, (e.g. Henderson *et al.,* 1999; Mandal and Rastogi 2005; Mandal *et al.,* 2005) it has been reported that the correlation can even change from a negative value to a positive one.

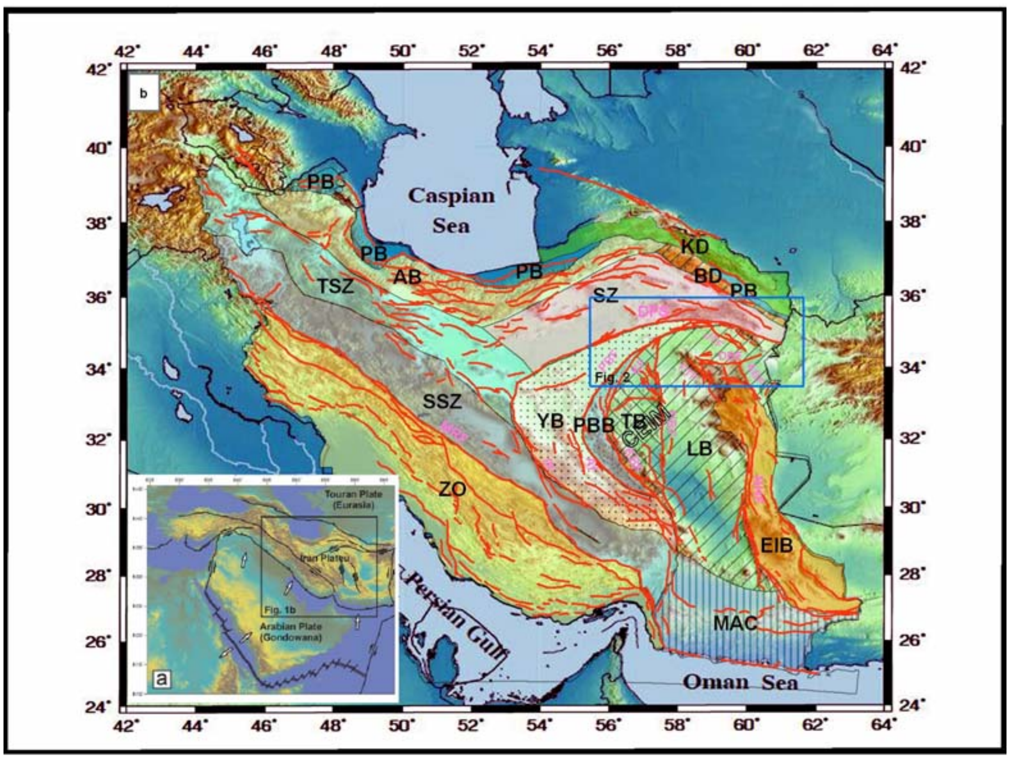

Figure 1. (a) Tectonic setting of Iran in the Middle East and presentation of major convergence vectors of the region. (b) Generalized tectonic map of Iran (modified from Alavi 1991, Hessami et al. 2003 and Aghanabati 2004). Abbreviations: AB, Alborz belt; ABF, Abiz fault; AF, Anar fault;BD, Binalud mountain range ; CEIB, Central –East Iranian Blocks; DBF, Dasht-e-bayaz fault; DF, Dehshir fault; DFS, Doruneh Fault System; EIB, East Iran belt; FTF, Ferdows Thrust fault; JTF, Jangal Thrust fault; KD, Kopeh Dagh; KF, Kalmard fault; KBF, Kohbanan fault; LB, Lut Block; MAC, Makran accretionary complex; MHF , Main Zagros Reverse Fault; NHF, Nehbandan fault; NBF, Nayband fault; PB, Paleo-Tethyan basin ; PBB, Posht-e-Badam Block;PBF, Posht-e-Badam fault; SZ, Sabzevar zone; SSZ, Sanandaj-sirjan zone; TB,Tabas Block; TSZ,Tabriz-Saveh zone; YB, Yazd Block; ZO, Zagros orogen. Box shows the North of Central –East Iranian Blocks (NCEIB) by fig. 2.

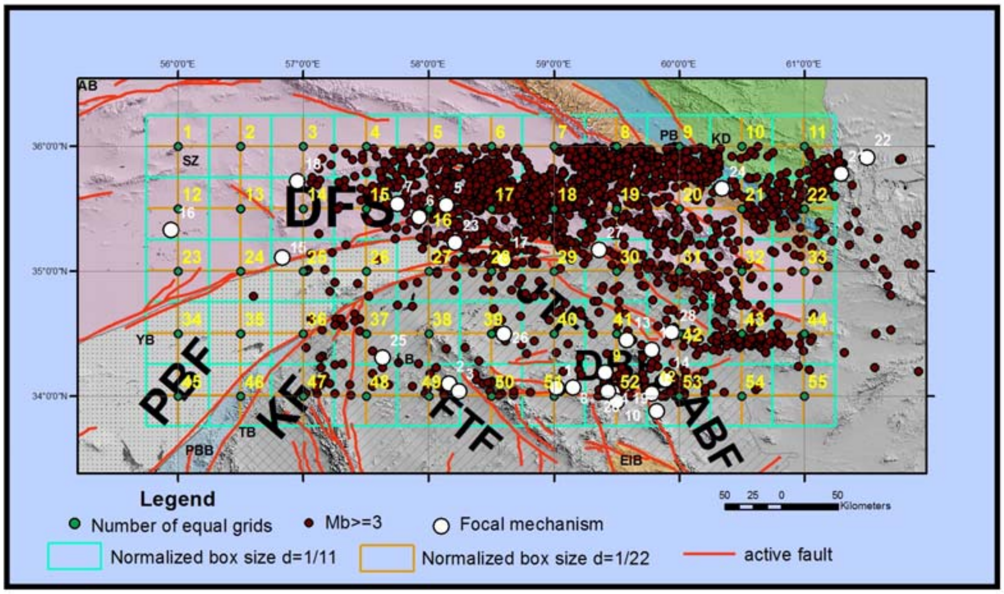

Figure 2. Epicenter distribution of earthquakes with Mb≥3 for instrumental period and 55 equal squares grid in the NCEIB. White points refer to focal mechanisms marked in table 1 and fig. 4. Normalized box size (d=1/s0) d=1/11 and (d=1/s1) d=1/22, Examples of the applications of the box-counting technique for measure fractal dimensions (Dc) map. "S" is increasing the area under calculation of Dc. The distribution is similar to that in Figure 1b.

We have computed the values of *a, b* and *Dc* for different seismogenic source zones of the NCEIB to determine the potential for earthquake hazard using analysis of seismicity during the instrumental period. We then produced maps for distribution of these parameters using different ranges and color scales. We then interpreted these values comparing them with seismicity, tectonic and seismotectonic properties of their related regions. We used the Least Squares (LSs) method to correlate these parameters.

Tectonic and geological setting

Cenozoic deformation in Iran is the result of the Arabian-Eurasia convergence that culminated in the Arabian Eurasia collision (Allen *et al.,* 2004; Agard *et al.,* 2011; Mouthereau *et al.,* 2012). The NCEIB is a major individual continental block within the collision zone between the Arabia and Eurasia which controls the distribution of strain in the northeastern part of the Iranian plateau (Naimi-Ghassabian *et al.,* 2015). This block is bounded by Doruneh fault system (DFS) to the north and Dasht-e-Bayaz fault zone to the south (Fig. 1).

The DFS is an intracontinental transform fault between the northern and southern sections of the CEIB defined above. The Doruneh fault is among the longest and most clearly traceable active faults in Iran which accommodates right-lateral shear between the CEIB and Afghanistan (Fathahi *et al.,* 2007; Zamani *et al.*, 2008). The northern domain of the DFS is consisted of outcrops of Paleozoic to Eocene rocks, while in the southern part Eocene rocks are overlain by more than 2000 m of Neogene-Quaternary deposits (Huber 1977; Alavi-naini *et al.,* 1992; Farbod *et al.,* 2011). Very few earthquakes epicenters have been recorded on or close to this fault despite the clear expression of its activity in morphotectonic and long term seismic activity (Ambraseys & Melville, 1982).

The low rate of seismic activity on the DFS is very different as compared to its relatively small counterpart, the Dasht-e-Bayaz fault zone in the south of study area. Dasht-e-Bayaz is a left-lateral strike-slip fault, which appears to play a major role in tectonics of the region (e.g. Walker & Jackson 2004) and forms the southern boundary of our study area (Fig. 1).

Some major active N-S striking right-lateral faults of the CEIB end near the DFS at latitude of about 34˚ N. Some authors (Jackson & McKenzie 1984; Walker and Jackson 2004; Allen et al. 2006; Fattahi et al. 2007) suggest that this right-lateral shear accommodates a clockwise block rotation on the E-W striking DFS and Dasht-e-Bayaz fault.

Farbod *et al.* (2011) proposed a model for the DFS, defining three distinct segments characterized by different kinematic regimes: the western

Doruneh fault system (WDFS), the central Doruneh fault system (CDFS) and the eastern Doruneh fault system (EDFS). The WDFS is characterized by earthquakes indicating left-lateral transpression, and some dome and basin structures within the folded Tertiary rocks in there are left-laterally offset. Most of the length of the WDFS cuts across the upper Miocene sandstones and marls (Upper Red Formation) with no major change in the topography across the fault zone. The Central Doruneh Fault Zone (CDFZ), is an east-trending almost pure left-lateral strike-slip fault system which separates the old reliefs of pre-Oligocene times to the north from the folded Neogene piedmont covered with Quaternary deposits to the south. To the south of the DFS are outcrops of moderately folded Miocene rocks. This is in contrast with the northern side, where intensely folded and faulted Paleozoic to Eocene sedimentary rocks which are intruded by the Upper Cretaceous to upper Eocene igneous rocks. The lack of Neogene sediments to the north of the DFS suggests that vertical component of faulting along the DFS in Oligocene and Miocene times affected the northern side of the sedimentary basin. This property makes the DFS different from the Great Kavir Fault, which cuts and offsets the post-Miocene structures within the Dasht-e-Kavir lowlands (e.g., Walker & Jackson, 2004), without any major sign for vertical faulting across the fault zone. This suggests the Oligo-Miocene Dasht-e-Kavir sedimentary basin continues on either side of the fault, and is not affected by vertical component of faulting across the Great Kavir Fault. The eastern Doruneh fault system (EDFS) is a trailing imbricate fan fault-termination characterized by reverse faulting and fault-related folding.

Methods

The empirical relationship between the frequency of earthquake events and their magnitudes is known as Gutenberg–Richter (G–R) law, which is expressed as the following formula:

$$\log N = a - bM \qquad (1)$$

Where N is the cumulative number of the events having a magnitude greater or equal to *M,* and *a* and *b* are constants representing the activity level of seismicity and the slope of the frequency–magnitude distribution respectively.

The relationship was first introduced by Gutenberg and Richter (1944) suggesting the constants then known as seismicity parameters. These parameters show significant variations in different regions because they depend on the seismic activity level, the period of observation, and the size of the considered area, as well as the size of the earthquake events. The *b* value reflects the relative frequency of the number of large and small earthquakes in a region. It is also dependent on the stress condition over the region. Several factors may perturb the normal value of *b*. The value is close to unity for most seismically active regions on the Earth (e.g. Frohlich & Davis, 1993). However, it normally varies between 0.5 and 1.5 (Pacheco *et al.,* 1992; Wiemer & Wyss, 1997). A detailed study of *b* value over large regions often reveals significant variations which is generally related to the distribution of stress and strain over the region (Mogi 1967; Scholz 1968). High *b* values are reported from areas with high geological complexity (Lopez Casado *et al.,* 1995), indicating the importance of multi fracture area. High heterogeneity in rock material or crack density results in high values of *b* (Mogi, 1962). On the other hand, low *b* value is related to low degree of heterogeneity, large stress and strain, large strain rate and large faults (Manakou & Tsapanos, 2000). The *b* values were first estimated by Gutenberg and Richter (1944) for different regions of the world. They suggested that *b* values vary from 0.45 to 1.50, while Miyamura (1962) found that *b* values range from 0.40 to 1.80 depending on the geological age of the studied area. Seismicity on a global scale has been studied by several authors, and it has been reported that *b* values vary between 1.0–1.6 (Mogi 1962), 0.8–1.2 (McNally 1989), 0.6–1.5 (Udias & Mezcua, 1997) and 0.53–1.19 (Bayrak *et al.,* 2002).

In order to evaluate the spatial distribution of *b* value in the study area, it is subdivided into a 0.5˚ ×0.5˚ grid (Fig. 2). The *b* values are calculated for circular epicentral areas centred at grid nodes. Radius of the circle to cover events across the grid is fixed (100km).

The fractal dimension, the Dc value, is calculated using the box-counting technique in order to measure 2-D fractal dimensions across the region. Analysis based on the box-counting is sensitive to a change in fractal dimension with scale (Blenkinsop, 1994; Blenkinsop & Sanderson 1999), however it is the most widely used. Grids with square boxes of spacing dimensions, d, are superimposed on the earthquake epicenters map, and the number of boxes containing earthquake epicenters, N_d, is counted (Fig. 2). The process is repeated for a defined range of values for d. On a log–log plot of N_d and d, a fractal earthquake epicenters pattern produces a straight line with a slope of –D, such that:

$N_d \alpha d^{-D}$ (2)

Where D is the fractal dimension (Turcotte 1992; Gillespie et al. 1993). Not all sizes are valid for the square boxes in box-counting analysis. Lower and upper scale limits exist to the curve which is obtained by the box-counting analysis. The upper limit corresponds to the largest value of box sizes at which no box contains more than one fracture, while the lower limit corresponds to the smallest value of box sizes at which all boxes contain one or more fractures. The relevant range indicates box sizes between those of the largest and the smallest fracture spacing (Walsh & Watterson 1993). The 2-D fractal dimension of fractures within the relevant box sizes should be in the range $1.0 < D < 2.0$ (Turcotte 1992).

The fractal dimension is used as a quantitative measure of the degree of heterogeneity of seismic activity for the fault systems of a region. It is controlled by the heterogeneity of the stress field as well as the preexisting geological, mechanical or structural heterogeneity (Öncel *et al.,* 1996; Bayrak & Bayrak 2012). Where the earthquakes become progressively more clustered, the value of *Dc* decreases (Öncel & Wilson 2002). The *b* value and *Dc* value change from region to region because of the variation in applied stress level over the regions.

The area of the present study is situated in the NCEIB, between 34°-36° N and 55°-61° E, and it was divided into 55 equal squares grid (fig. 2).

Results and discussions

Data and source zonation

Although earthquake catalogs cover a much shorter time period than paleosesmological, the earthquake records they provide are indispensable for seismic hazard analyses. In this study, we obtained several parameters necessary for evaluation of earthquake probability from earthquake catalog records. The methodology we used to evaluate the earthquake catalogs is based on the method proposed by Caceres and Kulhanek 2000 and Pailoplee *et al.* 2009.

We used earthquake data from the instrumental period between 1976 and 2015. The preliminary data were compiled from different sources and catalogs, which include GCMT (Global Centroid Moment Tensor catalogue available on line at: http:// www.globalcmt.org/CMTsearch.html), the earthquake catalogue at Iranian institute of Earthquake Engineering and seismology (on line at: http:// www.iiees.ac.ir), the earthquake catalogue at Iranian seismological center(on line at: http://irsc.ut.ac.ir/BPEI.php?lang=fa) and from the published literature (McKenzie 1972; Jackson and McKenzie 1984; Jackson *et al.* 2002; Fattahi *et al*. 2007; Shabanian *et al*. 2009; Farbod *et al*. 2011). These catalogs use different parameters such as magnitude scales (M_b: body wave magnitude, M_S: surface wave magnitude, and M_W: moment magnitude), origin time, epicenter and depth information of the earthquakes.

We then compiled a catalog which included homogeneous earthquake data resulted from conversion of different magnitude scales into Ms. The relationships among M_W, M_b and M_S are formulated in Eqs. (3-5) and are illustrated in (Fig. 3).

$Ms = 1.0265\ M_b + 0.0854 \quad R^2 = 0.9942$ (3)

$Mw = -0.0144\ M_b{}^2 + 0.7722\ M_b + 2.0106$
$R^2 = 0.9942$ (4)

$Mw= -0.0069\ M_S{}^2 + 0.7164\ M_S + 1.9934$
$R^2 = 0.9967$ (5)

Despite the fact that the M_W is usually used in recent seismic hazard assessments, we preferred to use the M_S magnitude in our study. Hanks and Kanamori (1979) suggest that M_W is calculated in a very similar manner as M_S for the earthquakes with $M_S \leq 8.0$. Besides, a major number of the earthquakes in the catalogs used in this study are reported based on M_S. Moreover, we have used the M_S magnitude scale because no earthquake with $M_S > 8.0$ have occurred in the study area during the instrumental period.

We divided The NCEIB into 55 equal square grids to carry out a more precise earthquake hazard analysis for the study region using an updated and more reliable version of earthquake catalog. In this catalog, only shallow earthquakes (h < 40 km) with an average depth of 20 km are used to evaluate the *b* and *Dc* values for the 55 regions defined for the study. The earthquake magnitudes range from 3 to 7.3 (5.2 on average) (Fig. 2).

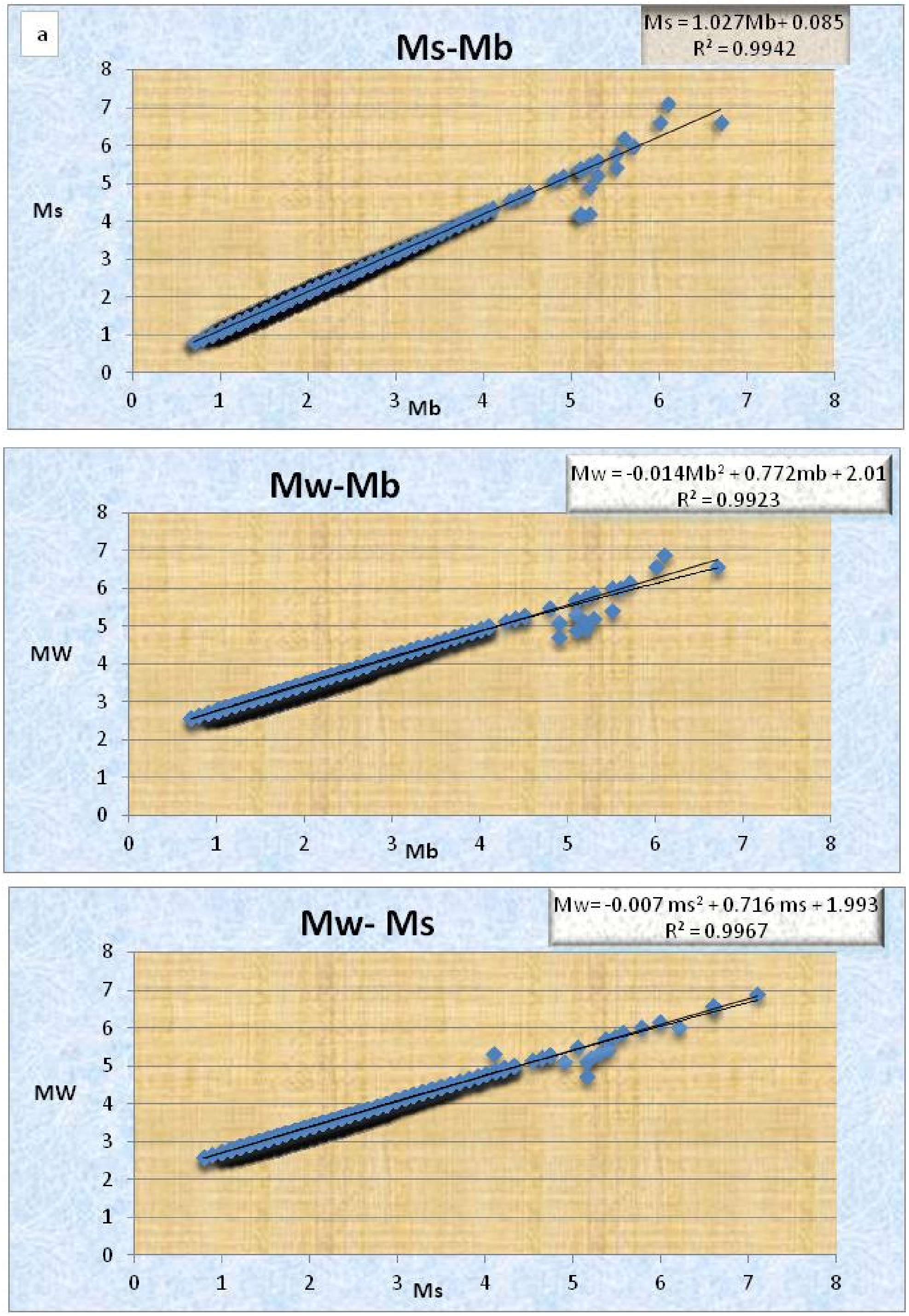

Figure 3. The relationships of MS, Mb and MW are formulated in Eqs. (3-5).

The epicenter distributions of the instrumental large earthquakes with known focal mechanism are listed in Table 1, fig. 2 and their characteristic are shown in Fig. 4. In this study, we used the earthquakes with M ≥ 4 showed in Fig. 2 to investigate regional variations of *b* and *Dc* values and relation between these parameters.

Frequency-magnitude distribution and Fractal dimension

In order to evaluate the seismicity dynamics of different 55 regions in the NCEIB during the instrumental period between 1976 and 2015, we calculated the G–R relationships and the fractal dimensions are computed.

To examine the spatial distribution of *b*, the study area is subdivided into a 0.5˚ ×0.5˚ grid. *b* values are calculated for circular epicentral areas centered at grid nodes.

Graphs showing the magnitude–frequency relationships are illustrated in Fig. 5, and the computed G–R parameters (*b* and *a* values) for 55 regions of The NCEIB are given in Table 2.

The b values are computed between 0.54 and 0.72. The lowest *b* values are found in the regions 9, 10, 11, 21and 22, whereas the highest are observed in the regions 16, 17, 18, 27, 28, 29 and 40.We divided *b* values into some groups, which are shown in fig. 6, and drawn with different color scale. The low *b* values may indicate a high-strain accumulation due to regional tectonics and stress build up over time, which may be released by earthquakes that are less in frequency but larger in magnitude (Öncel & Wilson 2002).

Graphs showing the fractal dimension are illustrated in Fig. 7, and the computed *Dc* values and their standard deviations for the 55 different regions of the NCEIB are given in Table 2. The computed *Dc* values which range between 0.125 and 1.07 suggest that the earthquake epicenters are evenly distributed over the whole region, and the study area is seismically active. The minimum *Dc* values belong to the regions 5, 7, 16, 25, 30 and 36, whereas the maximum values belong to the regions 3, 38, 52 and 53. We divided *Dc* values into some groups. These groups are illustrated using different color scales in Fig. 8.

In empirical terms, a *Dc* value close to 1 or 2 indicates that the earthquake epicenters are homogeneously distributed respectively along a line and over two-dimensional (2-D) fault plane.

The lowest *Dc* values (<1.5), indicate an active linear fault system (Yadav *et al.,* 2011).

Table 1. The large earthquakes parameters with known focal mechanisms in the NCEIB.
All angles are in degrees. (No.), site number refers to Fig. 2. The last column refers to the source of Focal mechanism; (B), Baker et al. (1993); (BY), Berberian and Yeats (1999); (J), Jackson et al. (2002); (JM), Jackson and McKenzie (1984); (H), Harvard catalogue during the period 1976–2015); (M), McKenzie (1972); (WJ), Walker and Jackson (2004).

No.	Date	Time	Lat.	Lon.	Mb	Ms	Mw	Depth	plane1			plane 2			Scalar-mom.	Ref.
	(yyyymmdd)	(hhmm)	(° N)	(° E)				(km)	Strike	Dip	Rake	Strike	Dip	Rake		
1	19680831	1047	34.07	59.02	6.2	7	7.1	17	254	84	5	320	70	90		W
2	19680901	0727	34.10	58.16	5.9	6	6.3	9	115	54	85					W
3	19680904	2324	34.04	58.24	5.3	5	5.5	9	148	56	81					W
4	19680911	1917	34.03	59.47	5.4	5	5.6	6	78	90	16					B
5	19710526	0241	35.53	58.14	4.8	5	5.4	26	88	26	31	329	76	112		JM
6	19721201	1139	35.43	57.92	4.8	5	5.4	33	156	65	-176	64	87	-25		J
7	19730517	1611	35.54	57.75	5.0	5	5.5	29	23	8	176	117	89	82		M
8	19761107	0400	34.07	59.15	5.6	6	6.0	15	260	78	6	169	84	168	1.09E+25	H
9	19790116	0950	34.19	59.41	6.7	6	6.5	15	267	49	5	174	86	139	6.75E+25	H
10	19790117	0951	33.96	59.50	6.0	7	6.5	13	257	88	5					B
11	19791114	0221	34.37	59.78	6.0	7	6.5	12	256	53	-1	347	89	-143	8.15E+25	H
12	19791114	0221	34.02	59.78	6.1	6	6.6	10	160	89	-177	85	85	1		B,J
13	19791127	1710	34.45	59.58	6.1	7	7.0	25	261	67	-19	358	73	-156	4.61E+26	H
14	19791207	0924	34.13	59.89	5.6	5	5.9	10	113	84	21					B
15	19791209	0912	35.11	56.83	5.2	5	5.6	15	350	44	121	129	53	63	2.81E+24	H
16	19880508	650	35.33	55.94	4.7	4	5.3	53	219	87	4	129	86	177		M
17	19941214	2044	35.09	58.60	5.1	4	5.2	33	319	32	144	80	72	63	8.47E+23	H
18	19960225	1614	35.72	56.95	4.8	5	5.4	33	82	77	10	350	80	166	1.42E+24	H
19	19970510	0757	33.88	59.82	6.5	6	7.2	13	156	89	-169					BER
20	19970625	1938	34.04	59.43	5.5	6	5.8	15	180	71	169	273	79	19	7.40E+24	H
21	19991109	0520	35.78	61.29	5.1	4	5.3	25	160	5	89	342	85	90	1.33E+24	H
22	19991205	1313	35.91	61.50	5.1	4	4.9	20	107	41	112	259	53	72	3.26E+23	H
23	20000202	2258	35.23	58.21	5.1	5	5.3	27	83	43	79	278	48	100	9.87E+23	H
24	20030703	1459	35.66	60.34	5.2	5	5.1	30	316	30	109	114	62	79	6.64E+23	H
25	20050531	0838	34.31	57.63	4.9	5	4.7	25	305	84	-1	39	89	-174	1.23E+23	H
26	20080703	2310	34.50	58.60	4.9	5	5.1	13	310	42	101	116	49	81	6.65E+23	H
27	20100730	1350	35.17	59.36	5.5	5	5.5	28	188	57	155	292	70	36	2.02E+24	H
28	20120701	2201	34.51	59.94	5.3	5	5.2	21	168	30	114	321	62	77	7.43E+23	H

Table 2. The Gutenberg–Richter (*a* and *b*), fractal dimension (*Dc*), *a/b* , Mb 50% (50% probability of exceedance in 50-year time period) and Dc/b parameters for 55 equal squares grid in the NCEIB.

Region N0.	LAT.	LON.	a	b	a/b	Mb(50%)	Dc	Dc/b
1	36.0	56.0	1.882	0.674	2.7921	5.6	0.4090	0.6069
2	36.0	56.5	1.826	0.668	2.7334	5.5	0.4048	0.6060
3	36.0	57.0	1.738	0.648	2.6819	5.6	0.6580	1.0154
4	36.0	57.5	1.798	0.665	2.7036	5.5	0.4027	0.6055
5	36.0	58.0	1.819	0.668	2.7229	5.5	0.1250	0.1871
6	36.0	58.5	1.775	0.662	2.6811	5.5	0.4010	0.6058
7	36.0	59.0	1.699	0.651	2.6096	5.5	0.2990	0.4593
8	36.0	59.5	1.518	0.627	2.4209	5.4	0.3823	0.6097
9	36.0	60.0	1.361	0.618	2.2021	5.2	0.3665	0.5931
10	36.0	60.5	1.092	0.593	1.8413	5.0	0.3406	0.5743
11	36.0	61.0	0.665	0.541	1.2290	4.7	0.3990	0.7375
12	35.5	56.0	1.611	0.650	2.4783	5.3	0.3864	0.5945
13	35.5	56.5	1.781	0.676	2.6344	5.4	0.3977	0.5883
14	35.5	57.0	1.707	0.686	2.4882	5.2	0.4250	0.6195
15	35.5	57.5	1.846	0.694	2.6598	5.3	0.3995	0.5757
16	35.5	58.0	2.048	0.716	2.8602	5.5	0.1250	0.1746
17	35.5	58.5	2.043	0.714	2.8612	5.5	0.4150	0.5812
18	35.5	59.0	1.984	0.706	2.8100	5.4	0.2210	0.3130
19	35.5	59.5	1.787	0.684	2.6124	5.3	0.3961	0.5791
20	35.5	60.0	1.657	0.663	2.4991	5.3	0.3879	0.5851
21	35.5	60.5	1.457	0.637	2.2871	5.2	0.3727	0.5850
22	35.5	61.0	1.281	0.613	2.0895	5.1	0.3580	0.5840
23	35.0	56.0	1.642	0.653	2.5144	5.4	0.3890	0.5958
24	35.0	56.5	1.681	0.658	2.5545	5.4	0.3919	0.5956
25	35.0	57.0	1.642	0.638	2.5735	5.5	0.1350	0.2116
26	35.0	57.5	1.850	0.677	2.7325	5.5	0.2990	0.4417
27	35.0	58.0	2.058	0.703	2.9273	5.6	0.4188	0.5957
28	35.0	58.5	2.156	0.715	3.0152	5.6	0.5020	0.7021
29	35.0	59.0	2.119	0.710	2.9843	5.6	0.4229	0.5956
30	35.0	59.5	1.953	0.690	2.8303	5.5	0.1750	0.2536
31	35.0	60.0	1.854	0.677	2.7384	5.5	0.3410	0.5037
32	35.0	60.5	1.699	0.661	2.5702	5.4	0.3931	0.5946
33	35.0	61.0	1.442	0.636	2.2671	5.2	0.3712	0.5837
34	34.5	56.0	1.590	0.643	2.4726	5.4	0.3860	0.6004
35	34.5	56.5	1.635	0.649	2.5191	5.4	0.3894	0.6000
36	34.5	57.0	1.658	0.638	2.6014	5.5	0.2530	0.3969
37	34.5	57.5	1.883	0.679	2.7738	5.5	0.4380	0.6451
38	34.5	58.0	2.077	0.703	2.9543	5.6	0.5340	0.7596
39	34.5	58.5	1.815	0.667	2.7217	5.5	0.4040	0.6056
40	34.5	59.0	2.119	0.713	2.9739	5.6	0.4221	0.5924
41	34.5	59.5	1.969	0.692	2.8452	5.5	0.4129	0.5966
42	34.5	60.0	1.884	0.681	2.7663	5.5	0.3580	0.5257
43	34.5	60.5	1.742	0.667	2.6115	5.4	0.3960	0.5937
44	34.5	61.0	1.492	0.643	2.3202	5.2	0.3751	0.5833
45	34.0	56.0	1.538	0.633	2.4295	5.4	0.3829	0.6049
46	34.0	56.5	1.589	0.640	2.4826	5.4	0.3867	0.6043
47	34.0	57.0	1.675	0.637	2.6293	5.5	0.4700	0.7378
48	34.0	57.5	1.917	0.681	2.8148	5.5	0.4107	0.6030
49	34.0	58.0	2.096	0.703	2.9813	5.6	0.4700	0.6686
50	34.0	58.5	1.475	0.619	2.3827	5.4	0.3410	0.5509
51	34.0	59.0	2.119	0.715	2.9635	5.6	0.4214	0.5893
52	34.0	59.5	1.985	0.694	2.8601	5.5	1.0700	1.5418
53	34.0	60.0	1.914	0.685	2.7940	5.5	0.8310	1.2131
54	34.0	60.5	1.785	0.673	2.6521	5.4	0.3990	0.5928
55	34.0	61.0	1.542	0.650	2.3721	5.2	0.3788	0.5828

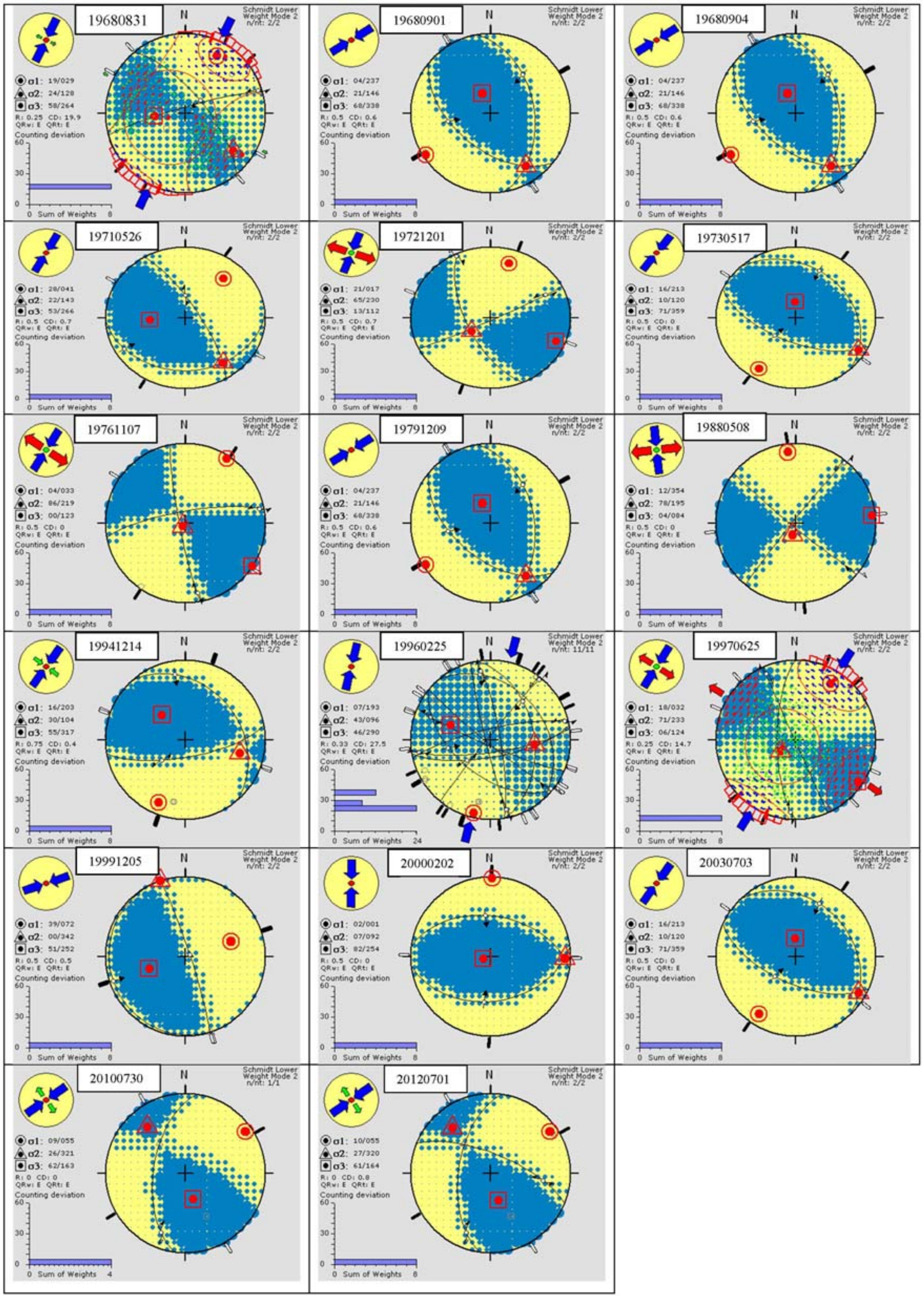

Figure 4. Focal mechanisms large earthquakes marked in table 1 in the NCEIB.

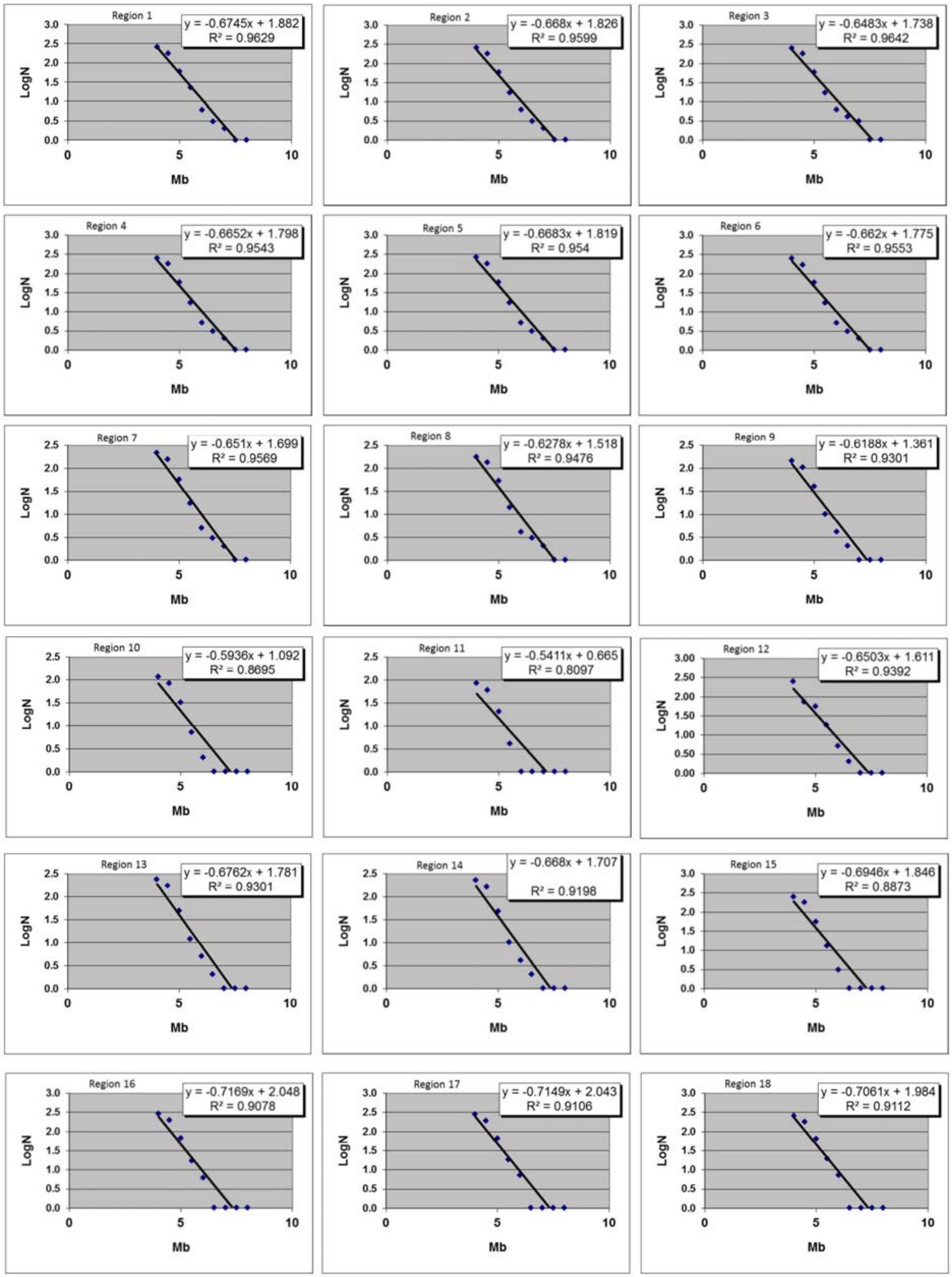

Figure 5. Continued on the next page

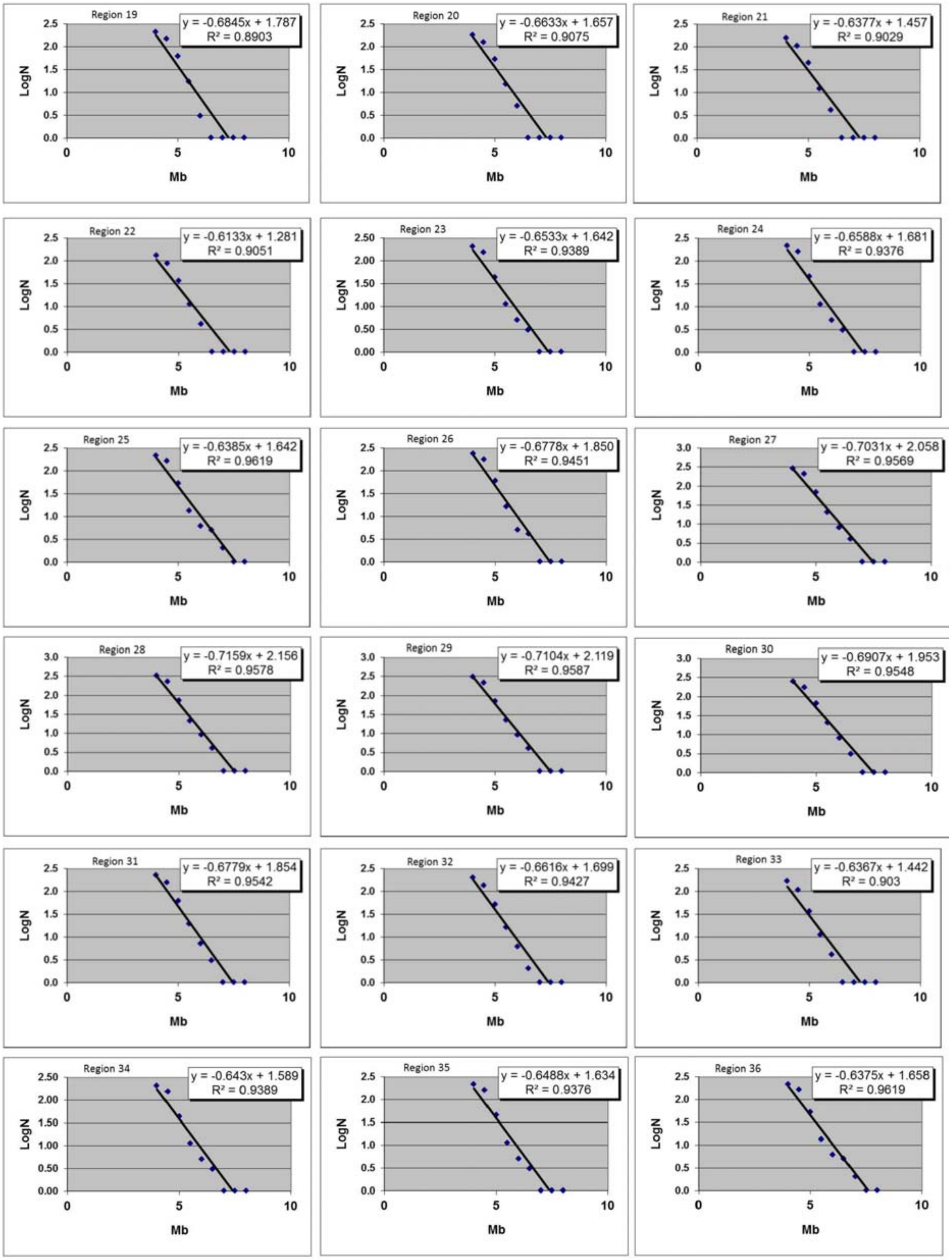

Figure 5. Continued on the next page

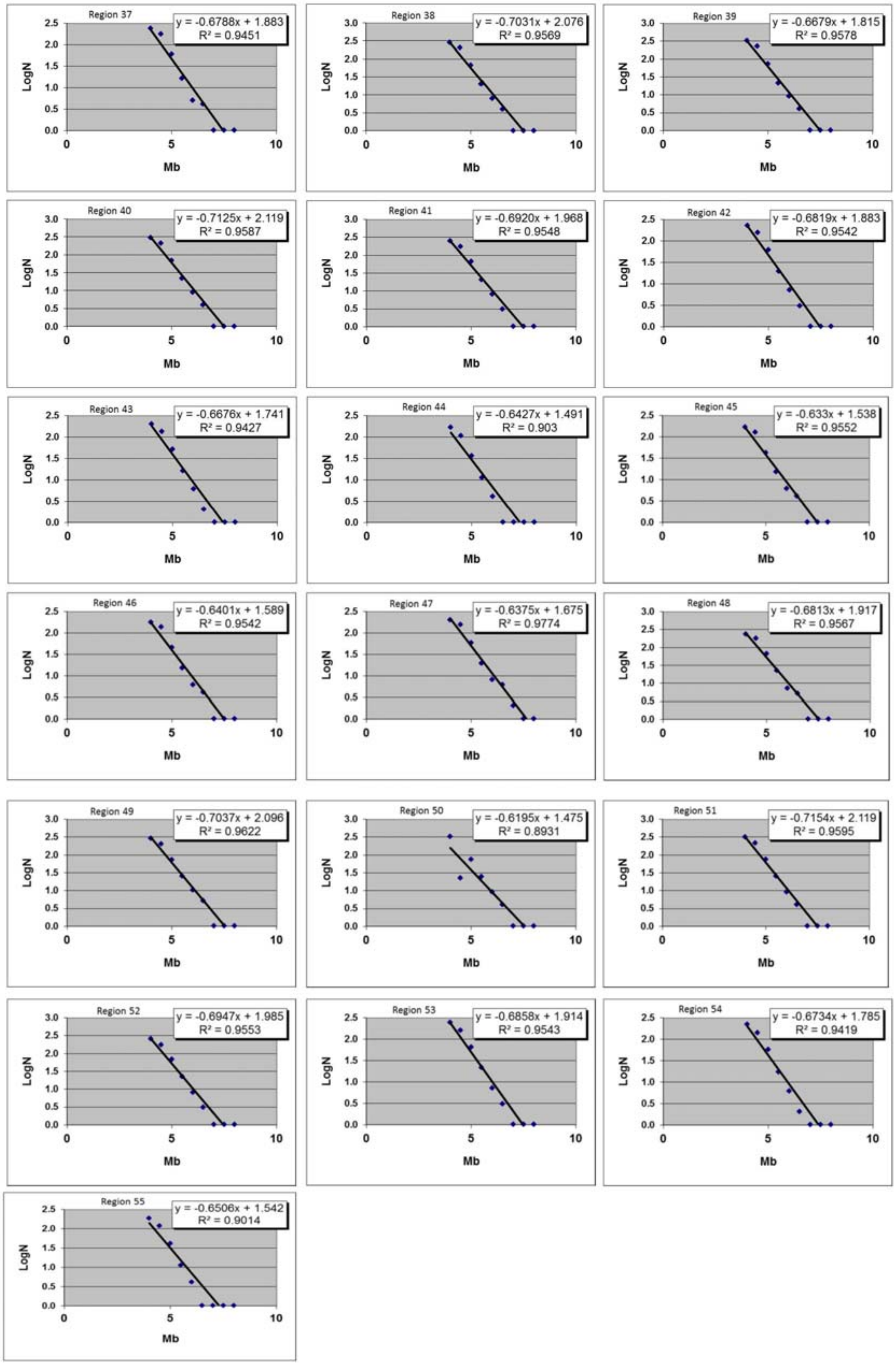

Figure 5. The Frequency-magnitude distribution (FMD) plots for 55 equal squares grid in the NCEIB. The lines represent the FMD linear regression fitted with the observed data

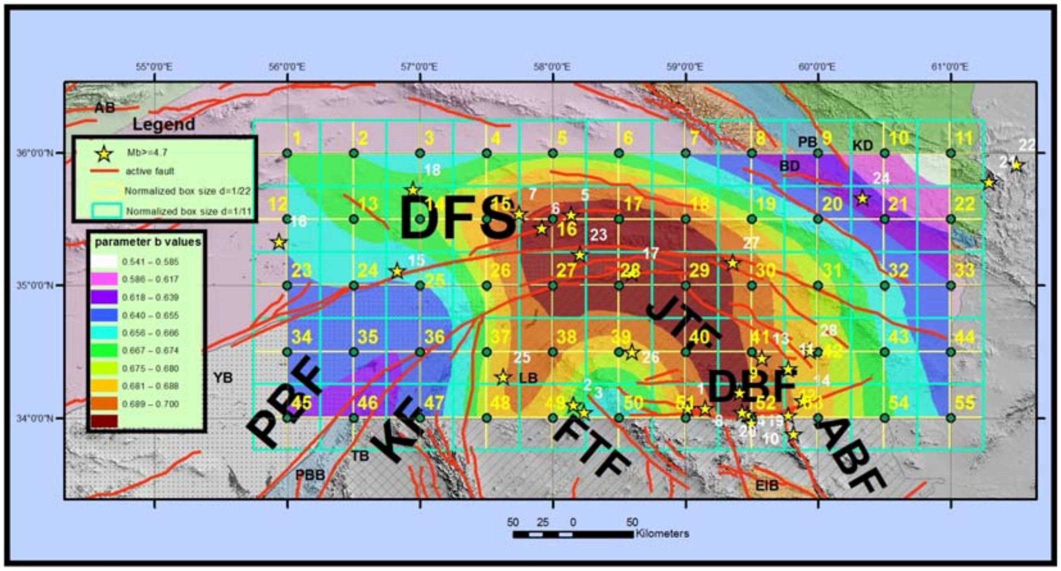

Figure 6. The computed b values for 55 equal squares grid in the NCEIB.

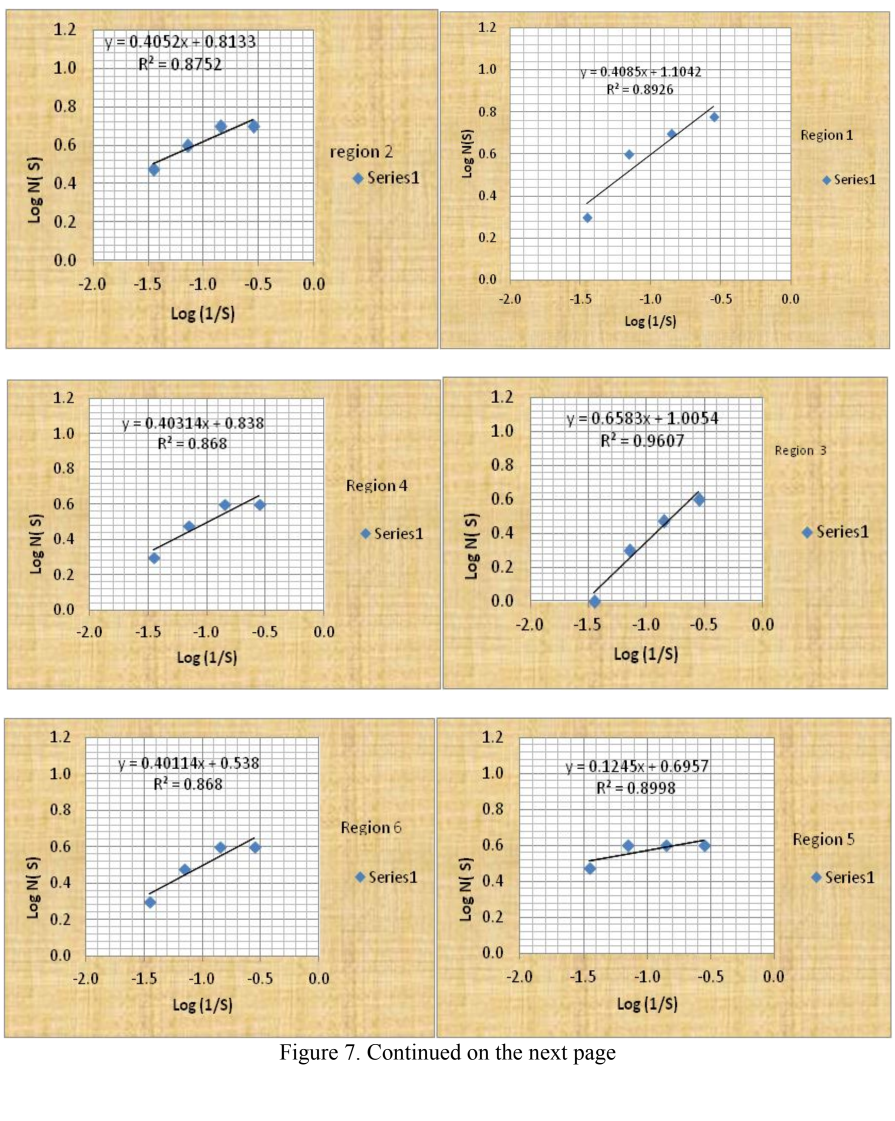

Figure 7. Continued on the next page

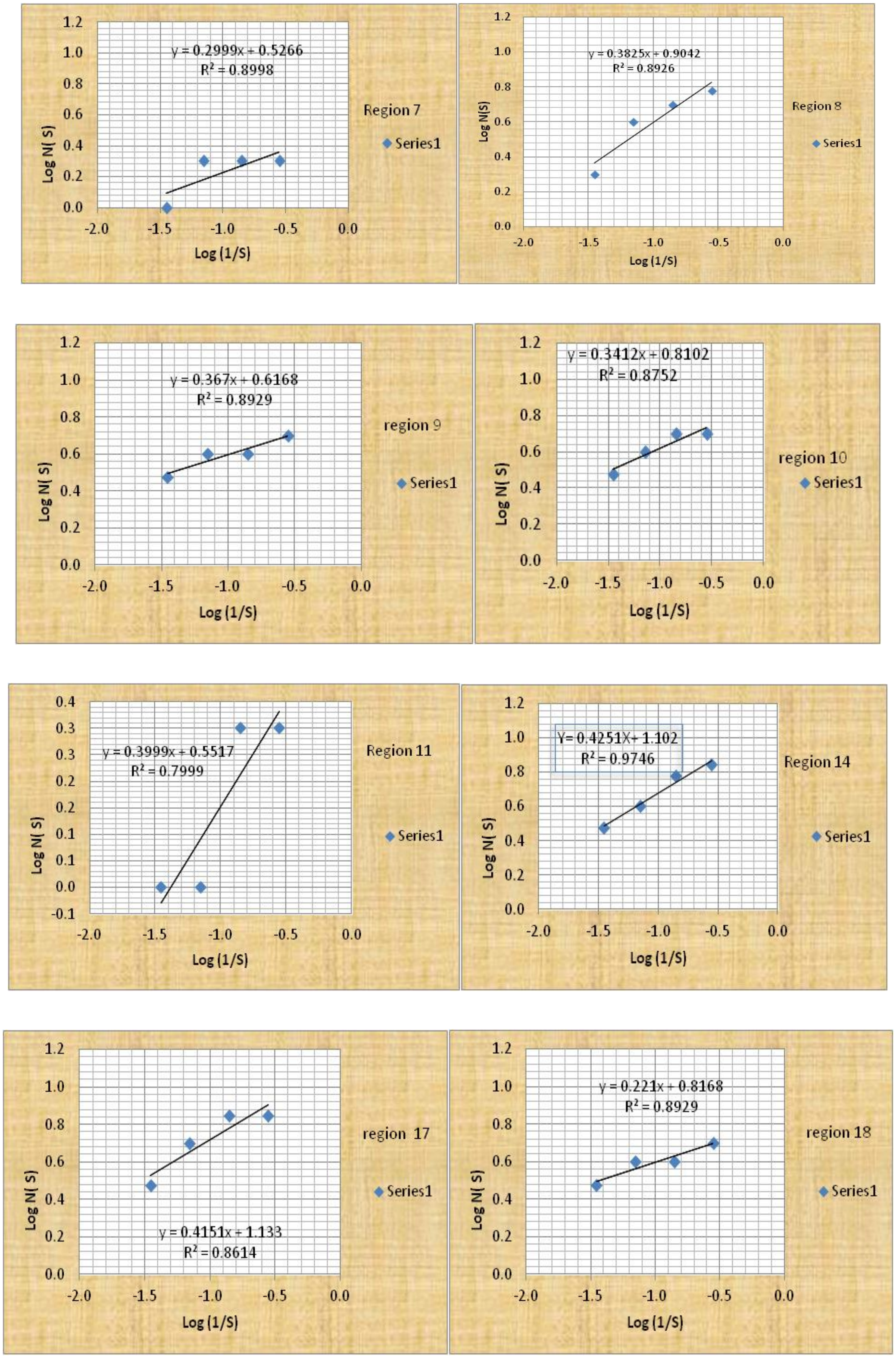

Figure 7. Continued on the next page

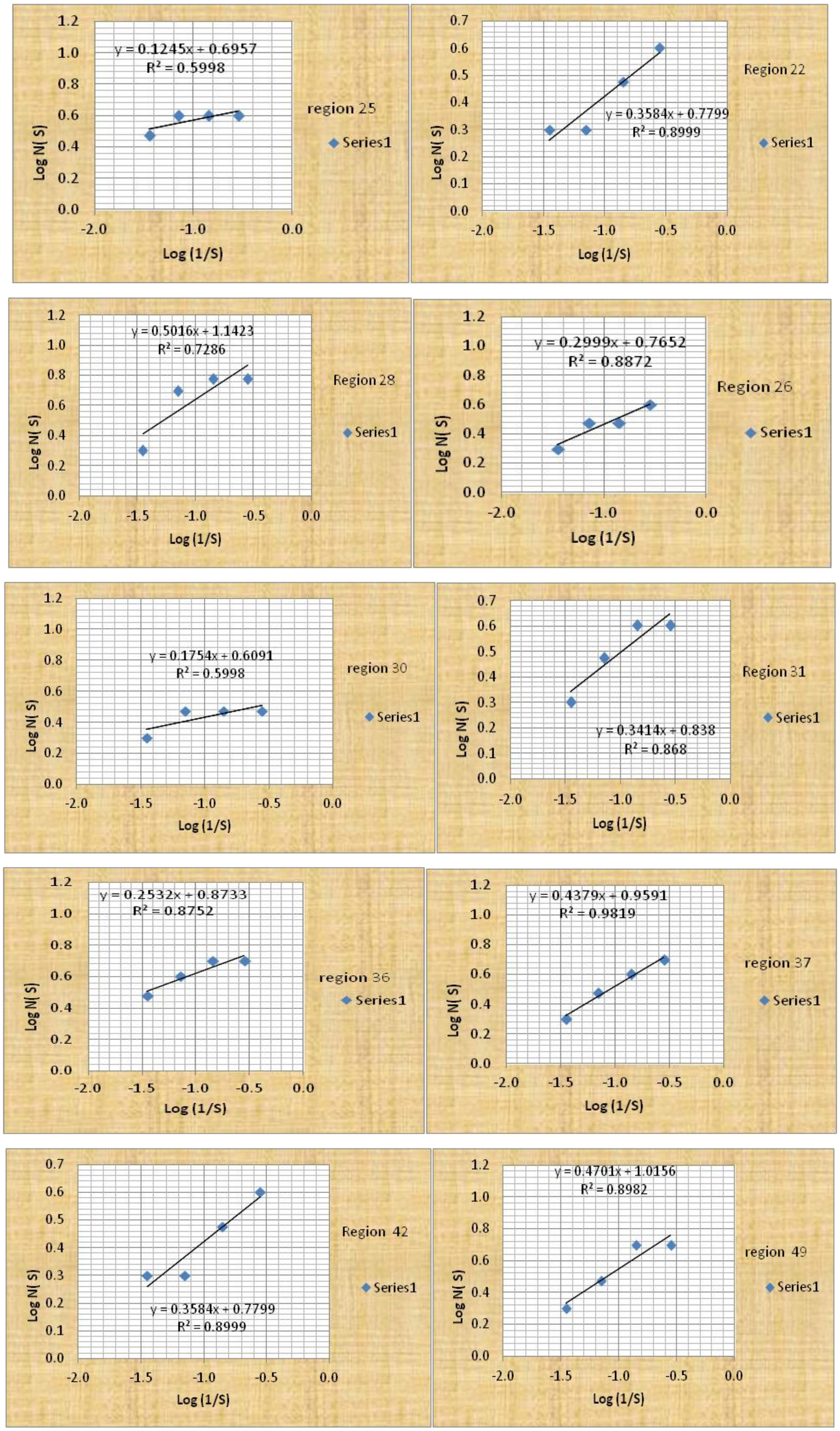

Figure 7. Continued on the next page

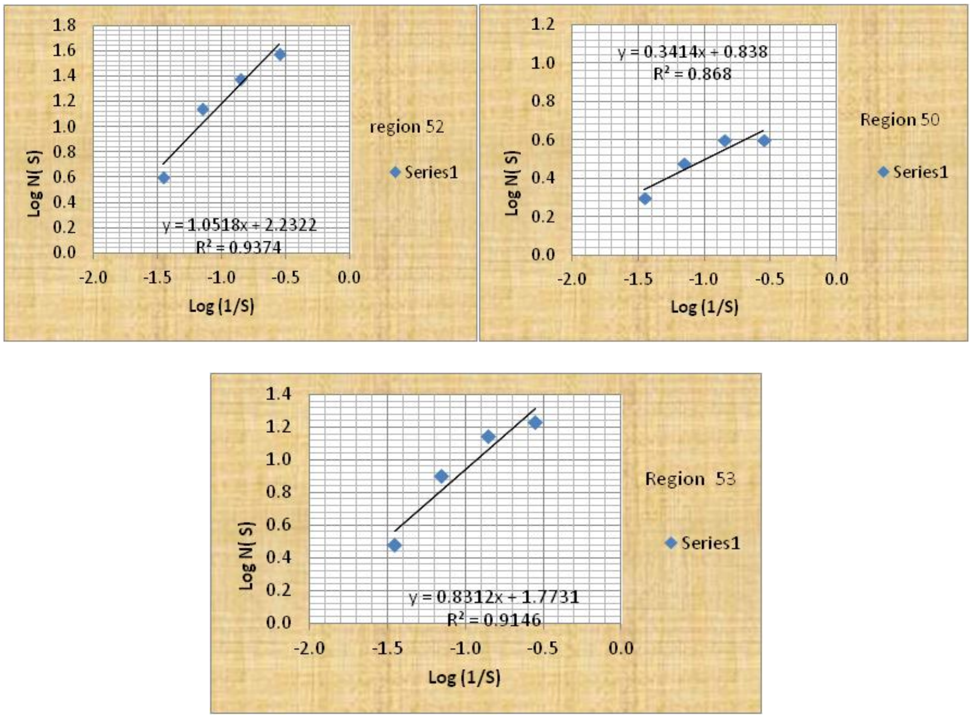

Figure 7. Graphs showing relationship between log N (S) and log (1/S) to determine fractal dimensions *(Dc)* for some equal squares grid in the NCEIB. "S" is increasing the area under calculation of Dc. The slopes of linear fit (solid black lines) are the fractal dimension (DC).See text and fig.2 for more information.

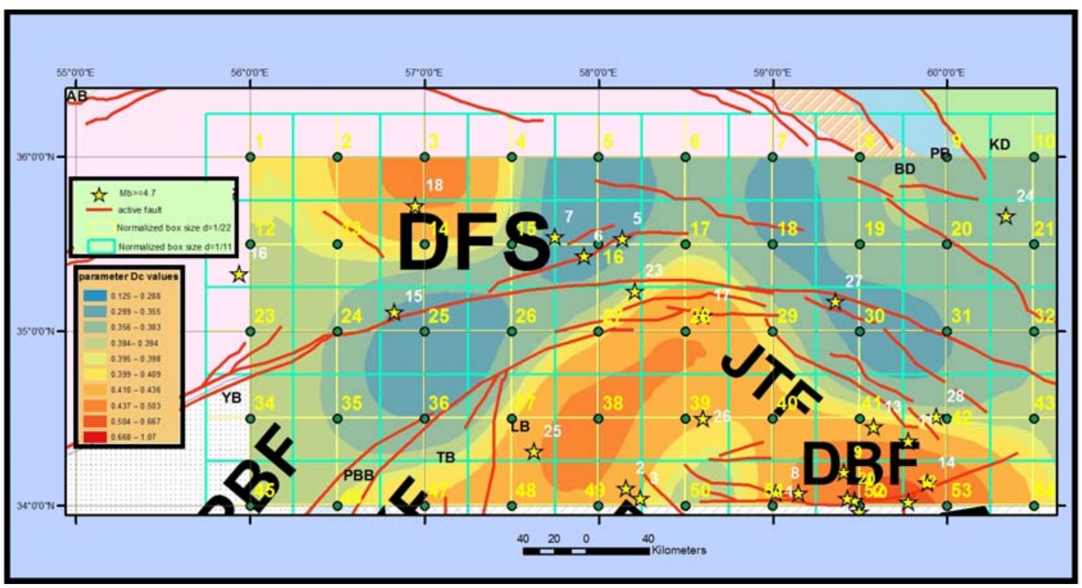

Figure 8. The computed parameter Dc values for 55 equal squares grid in the NCEIB. See text and fig.2 for more information.

We calculated the regression function (Fig. 9) for relationships between the *b* values and *Dc* values using the LS method;

$Dc = 0.609\, b - 0.008 \quad R^2 = 0.80$ (6)

Correlation coefficient (R^2) for this relationship is calculated to 0.60, showing positive correlation between the *Dc* and *b* values.

In empirical terms, the *Dc-b* correlation may be show either a positive or a negative regression. For example, positive regressions are reported for the San Andreas fault in the USA and some faults in India (Wyss *et al.,* 2004; Yadav *et al.,* 2012), whereas negative correlation are reported for some fault zones in Japan and Turkey (Hirata, 1989; Öncel *et al.,* 1996; Barton *et al.,* 1999; Öncel &

Wilson, 2002; Poroohan & Teimournegad, 2010; Bayrak & Bayrak, 2011, 2012).

According to the abovementioned relationships, in the NCEIB (Fig. 10), zones 16-18, 27-29 and 40 are defined as the regions with the highest stress, whereas zones 10, 11 and 22 show low stress accumulations. The calibration (Fig. 11) revealed a positive correlation as

$$Dc = 0.069\,(a/b) + 0.215 \qquad R^2 = 0.87 \qquad (7)$$

In Fig. (12), we computed *Dc* values based on Eq. 7.

A comparison between the Figs. 9 and 11 reveals that the distributions of both the *Dc*-*b* and Dc-(*a/b*) correlations are not significantly variant in terms of the data scatter.

Although Bayrak and Bayrak (2012) suggest that the Dc-(*a/b*) relationship is more reliable and effective than that of the Dc-*b* for indicating seismic hazards, both relationships in our study indicate an identical accuracy based on the R^2 values of 0.80 to 0.87. Therefore, both relationships between Dc-*b* and Dc-(*a/b*) could potentially reflect local seismicity and earthquake risk, and therefore may be useful in seismic hazard studies, particularly in the NCEIB.

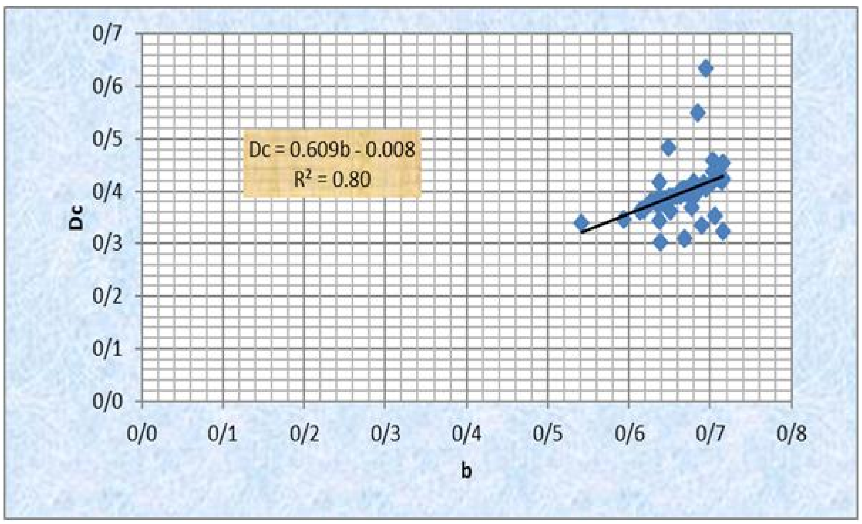

Figure 9. Empirical relationship between b and Dc values for 55 equal squares grid in the NCEIB. Straight line is the linear regression and r is the correlation coefficient.

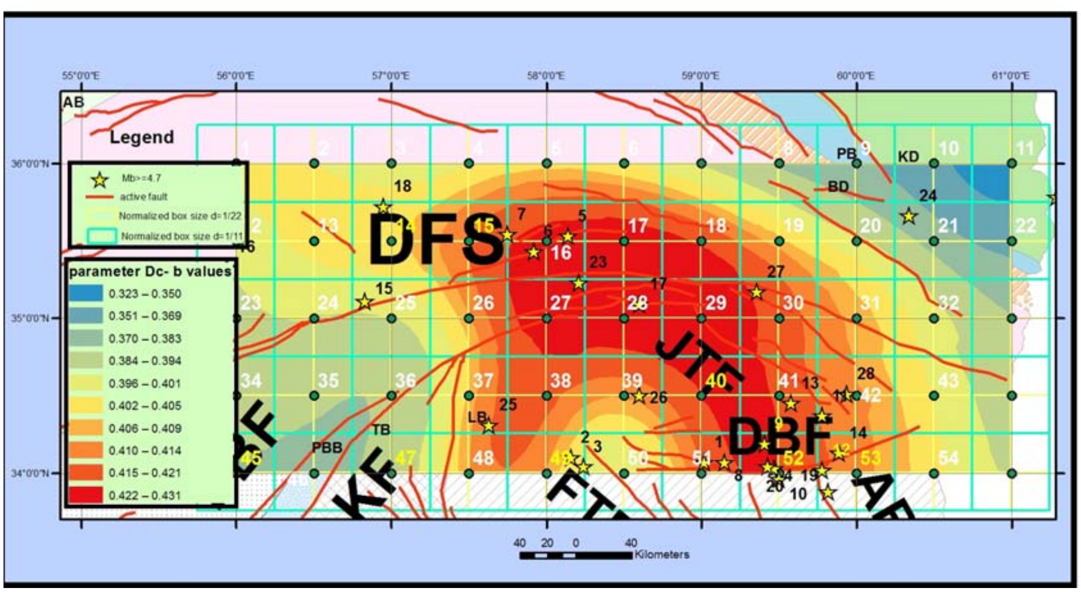

Figure 10. The computed parameter *Dc* values on the base of Eq. (6) for 55 equal squares grid in the NCEIB. .See text and fig.2 for more information.

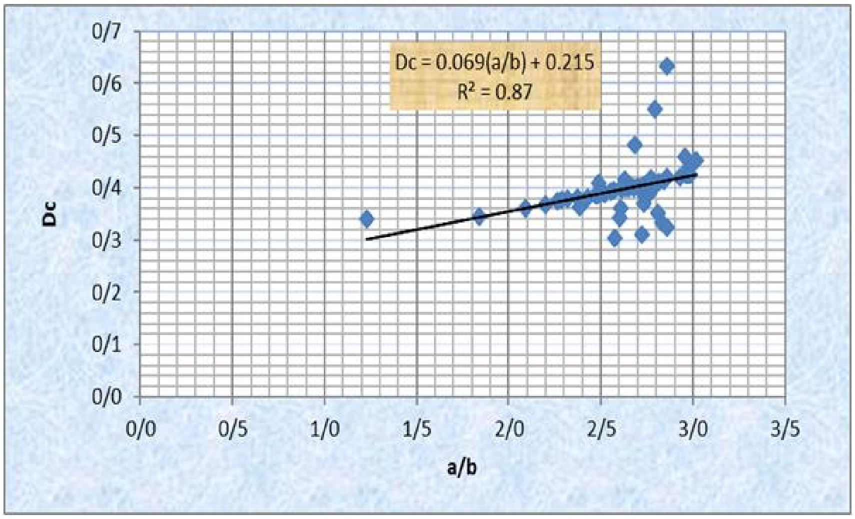

Figure 11. Empirical relationship between *a/b* and *Dc* values for 55 equal squares grid in the NCEIB. Straight line is the linear regression and r is the correlation coefficient.

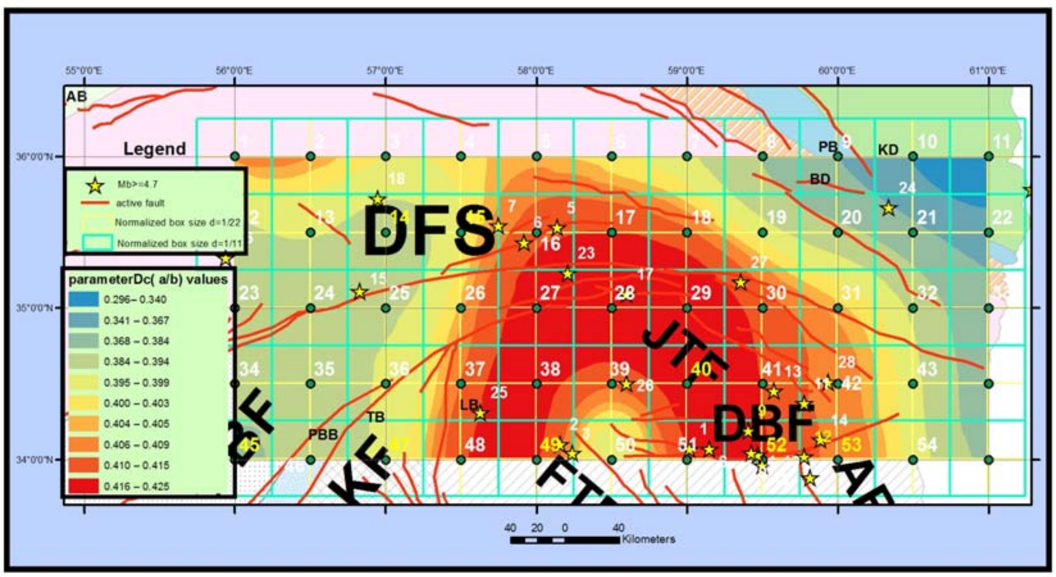

Figure 12. The computed parameter *Dc* values on the base of Eq. (7) for 55 equal squares grid in the NCEIB. See text and fig.2 for more information.

Dc/b relationship

The *Dc/b* ratio has been suggested as a useful indicator of seismic hazards in different regions, and it is possible that some large earthquakes occurred in past has increased the stress level and resulted in low *b* and high *Dc* values (Bayrak & Bayrak, 2011, 2012). The negative spatial correlation develops in response to an increase in stress concentration (lower *b*) and a decrease in epicenter clustering (increased *Dc*) (Öncel & Wilson, 2002).

Based on the obtained *Dc* and *b* values (Table 1) for the study area, the empirical *Dc/b* relationship is calibrated as shown in Fig. (13).

When a single earthquake epicenter *i is* considered to be a threat for the areas of interest, it is critical to select the appropriate frequency-magnitude model (i.e., probabilistic seismic hazard analysis (PSHA)) and activity rate. PSHA can be applied for preliminary evaluations or for risk analysis when these are unrelated to design decisions on a critical construction.

In this study, we obtained the probabilistic seismic hazard map for analyzing (PSHA) seismic hazards in the NCEIB (Fig. 14).

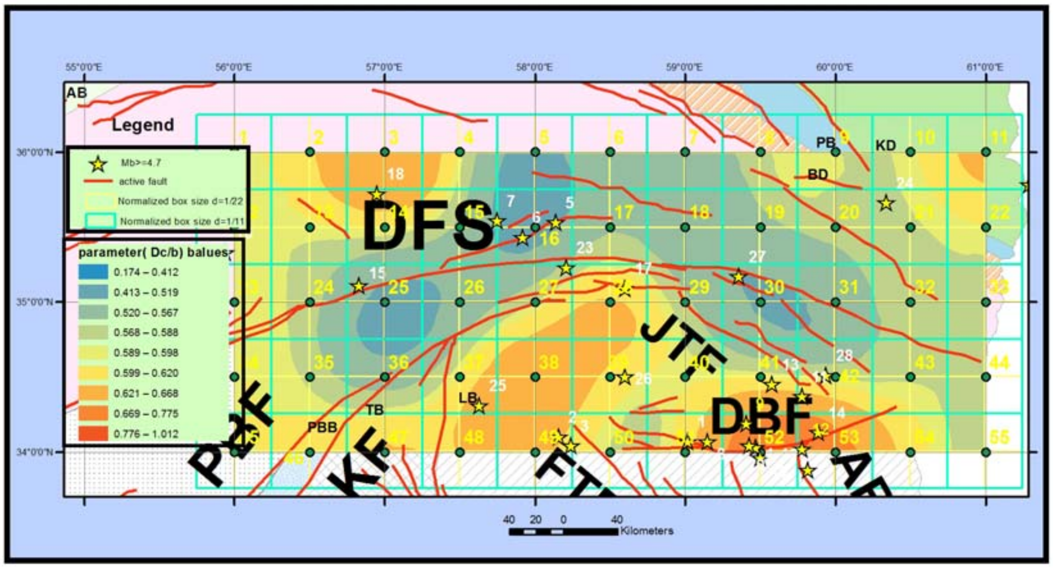

Figure 13. The map showing distribution of estimated parameter Dc/b values for 55 equal squares grid in the NCEIB. .See text and fig.2 for more information.

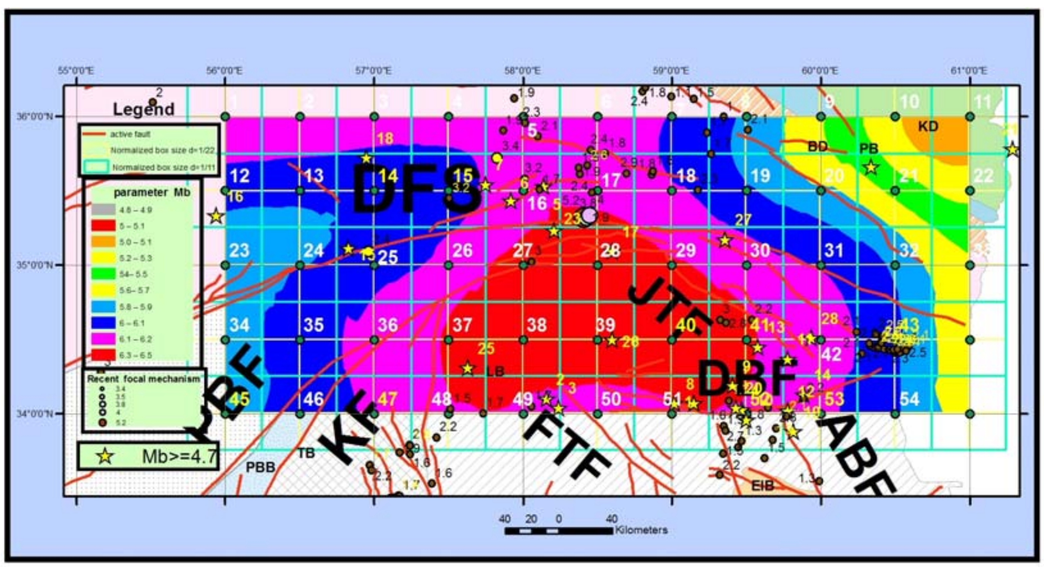

Figure 14. The probabilistic seismic hazard map of the NCEIB showing 10% probability of exceedance in 50-year time period. .See text and fig. 2 for more information.

Conclusions

We have analyzed and earthquake database which covers a period between 1976 and 2015 to study the regional distribution of the fractal dimension, Dc and G–R parameters (a and b) of the earthquake epicenters in 55 equal squares grids in the NCEIB to understand nature of the seismicity and the probability for the occurrence of a great earthquake in the region. We have employed the correlation integral method for estimation of Dc and the ML method for the G–R relationship. It is concluded that the regional variations in b and Dc values provide useful information about the state of stress within a zone. The lowest b-values and the highest Dc-values are observed in the central part of the NCEIB. We also observed high Dc/*b* values in the central part of the NCEIB. It is concluded that stress level is very high in the abovementioned region, and make them the most probable places for occurrence of large earthquakes in the NCEIB. We also conclude that *Dc/b* values may be used as indicators of earthquake hazard levels in different seismogenic zones in a region of interest. We examined the relationships between *Dc* and *b* values and between *Dc* and *a/b* values using the LS method. It indicates that the distribution of *a/b* and *Dc* values is less scattered as compared to the distribution of *b* and *Dc* values. We recommend using the relationship between *a/b* and *Dc* values together with relationship between *b* and *Dc* values for study of seismicity, earthquake risk and hazard studies considering the computed correlation coefficients for two relationships and the distributions of these parameters. The PSHA map (Fig. 14) is in good agreement with recent earthquakes in the NCEIB.

Acknowledgments

The authors are greatly indebted to J. Rowshanravan, the head of the Geological Survey of Iran, Northeast Territory, for providing facilities during this study. We are grateful to M.R. Ghasemi, A. Sloan, J. Hollingsworth, anonymous reviewers, and an Associate Editor for helpful and constructive reviews. The Editor-in-Chief, Dr. Ebrahim Ghasemi-Nejad, is acknowledged for help and editing the manuscript.

References

Agard, P., Omrani, J., Jolivet, J., Whiterurch, H., Vrielynck, B., Spakman, W., Monie, P., Meyer, B., Wortel, R., 2011. Zagros orogeny: a subduction-dominated process. Geological Magazine, 148: 692–725.

Aghanabati, A., 2004. Geology of Iran. Tehran, Geological Survey of Iran, 586 p. (in Persian).

Aki, K., 1981. A probabilistic synthesis of precursory phenomena. In: Simpson, D.W., Richards, P.G. (Eds.), Earthquake prediction: an international review, Maurice Ewing Set, vol. 4. AGU, Washington, DC, 566–574.

Alavi, M., 1991. Tectonic map of the Middle East (1:2900, 000). Geological Survey of Iran, Tehran.

Alavi-Naini, M., Vaezi-Pour, M. J., Alavi Tehrani, N., Behrouzi, A., Kholghi. M. H., 1992. Torbat-e Heidariyeh, in Geological Map of Iran, sheet K-5, scale 1:250,000, Geol. Surv. Of Iran, Tehran.

Allen, M., Jackson, J., Walker, R., 2004. Late Cenozoic reorganization of the Arabia-Eurasia collision and the comparison of short-term and long-term deformation rates. Tectonics, 23, TC2008. doi: 10.1029/2003TC001530.

Allen, M., Blanc, E.J.P., Walker, R., Jackson, J., Talebian, M., Ghassemi, M.R., 2006. Contrasting styles of convergence in the Arabia-Eurasia collision: Why escape tectonics does not occur in Iran. Geological Society of America Special Paper, 409: 579–89.

Ambraseys, N., Melville, C., 1982. A History of Persian Earthquakes, Cambridge Univ. Press, Cambridge, U. K, 240 p.

Baker, C., Jackson, J., Priestley, K., 1993. Earthquakes on the Kazerun Line in the Zagros Mountains of Iran: strike-slip faulting within a fold-and-thrust belt. Geo-phys. J. Int., 115 (1): 41–61.

Bayrak, Y., Yılmaztürk, A., Öztürk, S., 2002. Lateral variations of the modal (a/b) values for the different regions of the world. Journal of Geodynamics 34: 653–666.

Bayrak, Y., Bayrak, E., 2011. An evaluation of earthquake hazard potential for different regions in Western Anatolia using the historical and instrumental earthquake data. Pure Appl Geophys 169: 1859–1873.

Bayrak, Y., Bayrak, E., 2012. Regional variations and correlations of Gutenberg–Richter parameters and fractal dimension for the different seismogenic zones in Western Anatolia. J Asian Earth Sci. 58: 98–107.

Barton, D.J., Foulger, G.R., Henderson, J.R., Julian, B.R. 1999. Frequency-magnitude statistics and spatial correlation dimensions of earthquakes at Long Valley Caldera, California. Geophysical Journal International, 138: 563–570.

Berberian, M., Yeats, R.S., 1999. Patterns of historical earthquake ruptures in the Iranian Plateau. Bull. Seismol. Soc. Am., 89: 120–139.

Blenkinsop, T.G., 1994. The fractal distribution of gold deposits. In: Kruhl, J.H. (ed.), Fractals and Dynamic Systems in Geosciences. Kruhl, J.H. (ed.), Fractals and Dynamic Systems in Geosciences. Springer, Berlin, 247–258.

Blenkinsop, T.G., Sanderson, D.J., 1999. Are gold deposits in the crust fractals? A study of gold mines in the Zimbabwe craton. In: McCaffrey, K.J.W., Lonergan, L., and Wilkinson, J.J. (ed.), Fractures, Fluid Flow and Mineralization. Geological Society Special Publication, 155: 141–151.

Bott, M. H. P., 1959. The mechanisms of oblique slip faulting. Geol. Mag. 96: 109–117.

Caceres, D., Kulhanek, O., 2000. Seismic hazard of Honduras, Nat. Hazards, 22: 49–69.

Farbod, Y., Bellier, O., Shabanian, E., Abbassi, M.R., 2011. Geomorphic and structural Variations along the Doruneh Fault System (central Iran). Tectonics 30, TC6014. http://dx.doi.org/10.1029/2011TC002889.

Fattahi, M., Walker, R.T., Khatib, M.M., Dolati, A., Bahroudi, A., 2007. Slip-rate estimate and past earthquakes on the Doruneh fault, eastern Iran. Geophys. J. Int., 168, 691–709. doi:10.1111/j.1365-246X. 2006.03248. X.

Frohlich, C., Davis, S., 1993. Teleseismic b-Values: Or, Much Abouth 1.0. Journal of Geophysical Research 98: 631–644.

Gillespie, P.A., Howard, C.B., Walsh, J.J., Watterson, J., 1993. Measurement and characterisation of spatial distributions of fractures. Tectonophysics, 226: 113–141.

Guo, Z., Ogata, Y., 1995. Correlation between characteristic parameters of aftershock distributions in time, space, and magnitude. Geophysical Research Letters, 22: 993–996.

Gutenberg, B., Richter, C.F., 1944. Frequency of earthquakes in California. Bulletin of the Seismological Society of America, 34: 185–188.

Hanks, T.C., Kanamori, H., 1979. A moment-magnitude scale, J. Geophys. Res., 84: 2348–2350.

Henderson, J.R., Barton, D.J., Foulger, G.R., 1999. Fractal clustering of induced seismicity in the Geysers geothermal area, California. Geophysical Journal International 139: 317–324.

Hessami, K., Jamali, F., Tabassi, H., 2003. Map of Major Active Faults of Iran, Ministry of Science, Research and Tecnology, International Institute of Earthquake Engineering and Seismology (IIEES), Tehran, Iran.

Hirata, T., 1989. Fractal dimension of fault system in Japan: Fractal structure in rock fracture geometry at various scales. Pure and Applied Geophysics.

Huber, H., 1977. North Central Iran and North East Iran, in Geological Map of Iran, sheets 2 and 3, scale 1:1,000,000, Nati. Iranian Oil Co., Tehran.

Jackson, J., Mckenzie, D., 1984. Active tectonics of the Alpine-Himalayan Belt between western Turkey and Pakistan. Geophysical Journal of the Royal Astronomical Society, 77: 185–264.

Jackson, J., Haines, A., Holt, A., 1995. The accommodation of the Arabia–Eurasia plate

Convergence in Iran. Journal of Geophysical Research, 100: 15205–15219.

Jackson, J., Priestley, K., Allen, M., Berberian, M., 2002. Active tectonics of the South Caspian Basin. Geophys. J. Int., 148: 214–245.

Javadi, H. R., Ghassemi, M. R., Shahpasandzadeh, M., Guest, B., Esterabi Ashtiani, M., Yassaghi, A., Kouhpeyma, M., 2013. History of faulting on the Doruneh Fault System: Implications for the kinematic changes of the Central Iranian Microplate, Geol. Mag., doi: 10.1017/ S0016756812000751.

King, G.C.P., Nabelek, J., 1985. Role of fault bends in the initiation and termination of earthquake rupture, Science, 228, 984–987, doi: 10.1126/ science.228.4702.984.

Legrand, D., 2002. Fractal dimensions of small, intermediate, and large earthquakes. Bulletin of the Seismological Society of America 92, 3318–3320.

Lopez- Casado, C., Sanz de Galdano, C., Delgado, J., Peinado, M.A., 1995. The b parameter in the Betic Cordillera, Rif and nearbysectors. Relations with the tectonics of the region. Tectonophysics, 248: 277–292.

Manakou, M.V., Tsapanos, T.M., 2000. Seismicity and seismic hazard parameters evaluation in the island of crete and surrounding area inferred from mixed data files. Tectonophysics, 321: 157–178.

Mandal, P., Rastogi, B.K., 2005. Self-organized fractal seismicity and b value of aftershocks of the 2001 Bhuj earthquake in Kutch (India). Pure and Applied Geophysic, 162: 53–72.

Mandal, P., Mabawonku, A.O., Dimri, V.P., 2005. Self-organized fractal seismicity of reservoir triggered earthquakes in the Koyna-Warna seismic zone, western India. Pure and Applied Geophysics, 162: 73–90.

McKenzie, D., 1972. Active tectonics of the Mediterranean region. Geophys. J. R. Astron. Soc., 30: 109–185.

McNally, K.C., 1989. Earthquakes and seismicity. In: James, D.E., (Eds.), The Encyclopedia of Solid Earth. Geophysics, 308–315.

Miyamura, S., 1962. Magnitude–frequency relations and its bearing to geotectonics. Proc. Jpn. Acad. 38: 27–30.

Mogi, K., 1962. Magnitude-frequency relationship for elastic shocks accompanying fractures of various materials and some related problems in earthquakes. Bulletin of the Earthquake Research Institute University of Tokyo, 40: 831–883.

Mogi, K., 1967. Earthquakes and Fractures. Tectonophysics 5: 35–55.

Mouthereau, F., Lacombe, O., Vergés, J., 2012. Building the Zagros collisional orogen: timing, strain distribution and the dynamics of Arabia/Eurasia plate convergence. Tectonophysics, 532–535: 27–60.

Naimi-Ghassabian, N., Khatib, M.M., Nazari, H., Heyhat, M.R., 2015. Present-day tectonic regime and stress patterns from the formal inversion of focal mechanism data, in the North of Central-East Iran Blocks, Journal of African Earth Sciences, 111: 113–126.

Öncel, A.O., Main, I., Alptekin, Ö. Cowie, P., 1996. Temporal variations in the fractal properties of seismicity in the north Anatolian fault zone between 31_E and 41_E. Pure Applied Geophysics, 147: 147–159.

Öncel, A.O., Wilson, T., 2002. Space-time correlations of seismotectonic parameter and examples from Japan and Turkey preceding the izmit earthquake. Bulletin Seismological Society of America, 92: 339–350.

Öncel, A.O., Wilson, T., 2004. Correlation of seismotectonic variables and GPS strain measurements in western Turkey. Journal of Geophysical Research-American Geophysical Union, 109 (B11306): 1–13.

Pacheco, J.F., Scholz, C., Sykes, L., 1992. Changes in frequency–size relationship from small to large earthquakes. Nature, 355: 71–73.

Pascua, M.A.R., Devicente, G., Calvo, J.P., Perezlopez, R., 2003. Similarities between recent seismic activity and paleoseismites during the late Miocene in the external Betic Chain (Spain)-relationship by b value and the fractal dimension Journal of Structural Geology, 25: 749–763.

Pailoplee, S., Channarong, P., Chutakositkanon, V., 2013. Earthquake activities in the Thailand-Laos-Myanmar border region: a statistical approach. Terr Atmos Ocean Sci 24(Part II): 721–730.

Poroohan, N., Teimournegad, K., 2010. An analysis of correlations of seismotectonic parameter and fractal dimension preceding Roudbar-Tarom earthquake (northwest of Iran). Int Conf Geology Seismology, 148–154.

Scholz, C.H., 1968. The frequency–magnitude relation of microfracturing in rock and its relation to earthquakes. Bulletin of Seismological Society of America, 58: 399–415.

Shabanian, E., Siame, L., Bellier, O., Benedetti, L., Abbassi, M.R., 2009a. Quaternary slip-rates along the north-eastern boundary of the Arabia-Eurasia collision zone (Kopeh Dagh Mountains, north-east Iran). Geophys. J. Int., 178: 1055–1077

Shabanian, E., Bellier, O., Siame, L., Arnaud, N., Abbassi, M.R., Cochemé, J.J., 2009b. New tectonic configuration in NE Iran: Active strike-slip faulting between the Kopeh Dagh and Binalud mountains. Tectonics, 28, TC5002, doi: 10.1029/2008TC002444.

Tchalenko, J., Berberian, M., Behzadi, H., 1973. Geomorphic and seismic evidence for recent activity on the Doruneh fault, Iran. Tectonophysics, 19: 333–341.

Turcotte, D.L., 1986. Fractal model for crustal deformation. Tectonophysics 132: 261–269.

Turcotte, D.L., 1992. Fractals and Chaos in Geology and Geophysics. Cambridge University Press, Cambridge, 221 p.

Vernant, P., Nilforoushan, F., Chery, J., Bayer, R., Diamour, Y., Masson, F., Nankoli, H., Ritz, F., Sedighi, M., Tavakolim, F., 2004a. Deciphering oblique shortening of central Alborz in Iran using geodetic data. Earth Planet. Sci. Lett., 223(1–2): 177–185.

Vernant, P., Nilforoushan, F., Hatzfeld, D., Abbassi, M.R., Vigny, C., Masson, F., Nankali, H., Martinod, J., Ashtiani, A., Bayer, R., Tavakolim, F., Chéry, J., 2004b. Present-day crustal deformation and plate kinematics in the Middle East constrained by GPS measurements in Iran and northern Oman. Geophysical Journal International, 157: 381–398.

Udias, A., Mezcua, J., 1997. Fundamentos de Geofisica. Alianza Universidad Textos Paper no. 476.

Walker, R., Jackson, J., 2004. Active tectonics and Late Cenozoic strain distribution in central and eastern Iran. Tectonics, 23, TC5010, doi: 10.1029/2003TC001529.

Walsh, J.J., Watterson, J., 1993. Fractal analysis of fracture patterns using the standard box-counting technique: valid and invalid methodologies. Journal of Structural Geology, 15: 1509–1512.

Wang, J.H., 1991. A note on the correlation between b-value and fractal dimension from synthetic seismicity, Terrest. Atmospheric and Oceanic Sciences 2: 317–329.

Wang, J.H., Lee, C.W., 1996. Multifractal measures of earthquakes in west Taiwan. Pure and Applied Geophysics, 146: 131–145.

Wiemer, S., 2001. A software package to analyze seismicity: ZMAP. Seismological Research Letters 72: 373–382

Wiemer, S., Wyss, M., 1997. Mapping the frequency–magnitude distribution in asperities: an improved technique to calculate recurrence times. Journal of Geophysical Research 102: 15115–15128.

Wyss, M., Sammis, C.G., Nadeau, R.M., Wiemer, S., 2004. Fractal dimension and bvalue on creeping and locked patches of the San Andreas fault near Parkfield, California. Bulletin of Seismological Society of America, 94: 410–421

Zamani, B., Angelier, J., Zamani, A., 2008. State of stress induced by plate convergence and stress partitioning in northeastern Iran, as indicated by focal mechanisms of earthquakes. J. Geodyn. 45: 120–132. doi:10.1016/j.jog.2007.07.003.

Yadav, R.B.S., Papadimitriou, E.E., Karakostas, V.G., Rastogi, B.K., Shanker, D., Chopra, S., Singh, A.P., Kumar, S., 2011. The 2007 Talala, Saurashtra, western India earthquake sequence. Tectonic implications and seismicity triggering. Journal of Asian Earth Sciences, 40 (1): 303–314.

Yadav, R.B.S., Gahalaut, V.K., Chopra, S., Shan, B., 2012. Tectonic implications and seismicity triggering during the 2008 Baluchistan, Pakistan Earthquake Sequence. Journal of Asian Earth Sciences, 45 (2): 167–178.